https://doi.org/10.22226/2410-3535-2022-2-89-93

Thermokinetics of shape recovery of nanostructured titanium nickelide

E. P. Ryklina†, D. A. Ashimbaev, S. R. Murygin

†ryklina@tmo.misis.ru

Metal Forming Department, National University of Science and Technology MISIS, Moscow, 119049, Russia

The microstructure, martensitic transformations (MTs), functional characteristics and thermokinetics of shape recovery of Ni-rich titanium nickelide was studied. Post-deformation annealing at a temperature of 823 K (30 min) after cold drawing with the accumulated logarithmic strain of 0.6 forms a mixed nano-sized grain/subgrain structure of B2 austenite. The training procedure was carried out using isothermal and non-isothermal bending modes. The loading-unloading temperatures were associated with the characteristic temperatures of MTs; the loading strain was varied in the range of 13–19%. The specific features of the evolution of functional characteristics when using various loading modes are described. The strain-temperature conditions for the realization of the total shape recovery 17% and TWSME value 4% are revealed. The two-stage character of shape recovery after unloading is revealed; the hypothesis of its origin is suggested. The start and finish temperatures of shape recovery vs loading strain are measured. When using the non-isothermal mode with deep cooling under load, the temperature range for shape recovery expands from 35 to 77 K with increasing loading strain. When using the isothermal mode with loading-unloading at a start temperature of the direct MT, the temperature range of shape recovery degrades from 66 to 54 K.

Keywords: titanium nickelide, nanostructure, martensitic transformations, thermokinetics of shape recovery, temperature range of shape recovery.

1. Introduction

The unique functional properties of the Ni-rich titanium nickelide remain unsurpassed among the shape memory alloys (SMAs). A great attention to the nanostructured Ti-Ni alloys is caused by a combination of high mechanical properties and shape recovery characteristics [1–6]. To induce the shape memory effect (SME) as well as the two-way SME (TWSME), at least a single training cycle is required. The training procedure initiates martensitic transformations under loading and results in the increase of the defect density. These structural changes determine the behavior of an alloy in the process of subsequent shape recovery. The initial phase state (associated with loading-unloading temperatures) and loading strain strongly affect the shape recovery characteristics of Ni-rich titanium nickelide [7–10]. In [4,7,8], the authors revealed the possibilities to realize an abnormally high shape recovery value (15–17%) in Ni-rich titanium nickelide using various training modes. The systematic studies for control of the TWSME value (positive and negative) were carried out in [9,10]. It was proved in [7–10] that variation of the initial phase state (B2 austenite, R, and B19' martensite and their combination) when training appears a powerful tool for precise regulation of shape memory and superelasticity effects of Ni-rich titanium in a wide range of the structure types. The accumulated experience in practical use, particularly for designing medical devices shows, however, that the required shape recovery value and TWSME value amounts 3–5% and 1–2% respectively [11–14] in the desired temperature range. In this situation, the most important task remains to ensure the required temperature range as well as thermokinetics of shape recovery. The possibilities of the control of these important characteristics have not yet been studied before. To fill this gap seems an acute and necessary task. The revealed possibilities would be useful as well as in the case of deviation from the desired alloy composition. The present work aims to reveal the effect of external action, namely the initial phase state and loading strain on thermokinetics and the temperature range of shape recovery in Ni-rich titanium nickelide.

2. Experimental Procedure

The studies were carried out using a 0.45 mm diameter wire of Ti-50.8 at.% Ni titanium nickelide supplied by "MATEK-SMA" (Russia). The wire was obtained as a result of a multipass cold drawing with an accumulated strain of $e = 44\%$ (a true logarithmic strain of $e = 0.6$). The wire was cut into 50 mm long samples; post-deformation annealing (PDA) was performed at a temperature of 823 K, 30 min.

The structural studies were carried out using a JEM-2100 transmission electron microscope (TEM) operated at 200 kV. The foils were cut off the middle of the wire samples using a scanning ion microscope "Strata FIB 205" by local precision ion etching, with accelerating voltage of a focused ion beam of 30 kV. The calorimetric studies of the martensitic transformations (MTs) were carried out using a "Mettler Toledo 822e" calorimeter at a rate of 10 K/min in the range of 173 to 373 K. The start and finish temperatures of MT were determined using the ASTM F2004-05 (2010) standard.

The training procedure was carried out using a bending mode. Loading (total) strain ε_t was varied in the range of 13–19% (using the cylindrical mandrels of various diameters); its value was calculated as: $\varepsilon_t = d/(d+D)$ (where d — the wire diameter, mm, D — the diameter of a mandrel, mm, see Fig. 1).

The recovery strain ε_r and the TWSME value were calculated using a measured angle θ: $\varepsilon_r = [(180° - \theta_f)/180] \times \varepsilon_t$; $\varepsilon_{TW} = [(\theta_f - \theta_{TW})/180] \times \varepsilon_t$ (where θ_f — a residual angle after heating; θ_{TW} — an angle after cooling; ε_{TW} — the TWSME value). An angle θ was measured using a tangent method in the Compass-3D program.

The total recovery strain includes the recovery strain (ε_r) and the elastic strain (ε_{el}): $\varepsilon_r^{tot} = \varepsilon_r + \varepsilon_{el}$.

The interrelations between shape recovery characteristics are given in [15]. The loading-unloading temperatures were associated with the characteristic temperatures of MTs. Mode 1 includes the following steps: heating to 373 K → cooling to a temperature R_s (the start temperature of B2→R transformation) → loading → cooling under a constant strain to 77 K → unloading → heating. Mode 2 includes the following steps: heating to 373 K → cooling to a temperature M_s (the start temperature R → B19' transformation) → loading → unloading → heating. Before loading each sample was heated up to 373 K; subsequent cooling ensures the hit into the chosen start transformation temperature (R_s and M_s). In all cases, the exposure time under loading temperature and before unloading (in case of Mode 1) was 30 sec.

3. Results and Discussion

The cold drawing with the accumulated logarithmic strain of 0.6 forms a developed dislocation substructure (Fig. 1). A characteristic halo in the selected area diffraction pattern (SAED) indicates a partial amorphization (≈30%) of the structure (Fig. 2 a). Diffraction arcs (100) and (110) belong to B2-austenite; the weak reflections of B19'-martensite (122) are visually detected at high magnification. PDA at a temperature of 823 K (30 min) forms a mixed structure of recrystallized nanograins and nanosubgrains of the polygonized substructure of B2 austenite; their fractions are comparable, and the average size does not exceed 90 nm. In the SAED, the superposition of arc reflections from the nano-subgrains and point reflections from nano-sized grains distributed over a ring are observed, the reflections of the B2(110) and B19'(112) are detected. It is believed that

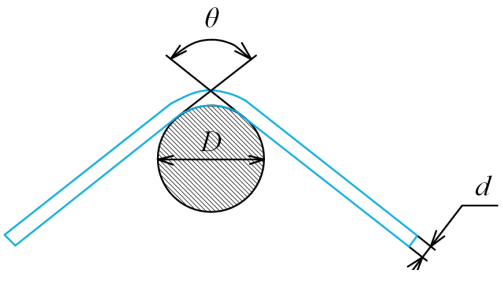

Fig. 1. The measured parameters for calculation of shape recovery characteristics: d and D — a sample and a mandrel diameter respectively; θ — an angle between straight tips of a sample.

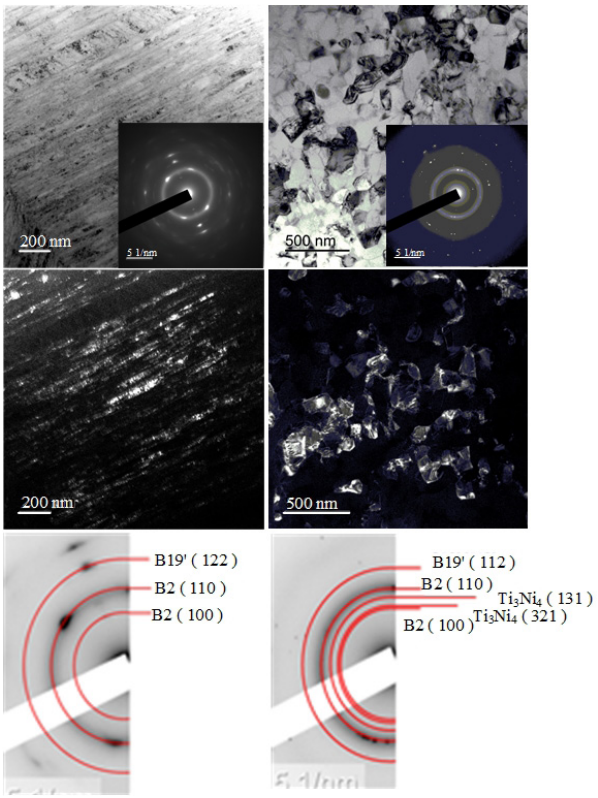

a b

Fig. 2. TEM microstructure: after cold drawing with accumulated strain of 0.6 (a); after PDA at 823 K, 30 min (b).

aging is suppressed at this temperature, nevertheless, the reflections (321) of Ti_3Ni_4 precipitates are also detected; their interpretation was performed using data of [16–18].

The calorimetric curves show two distinct exothermic peaks upon cooling: B2→R at 277 K and R→B19' at 221 K (Fig. 3). The start temperatures of the direct MTs amounts to 281 K (R_s) and 231 K (M_s). These temperatures were chosen as loading temperatures for modes 1 and 2 respectively. Upon heating, one peak is recorded at a temperature of 282 K, corresponding to a continuous reverse MT B19'→(R)→B2. The proceeding of the reverse MT through R-phase in the same alloy after aging was proved in [19] using X-ray study. The temperature route of training modes described above is plotted on the same pictures.

The diagrams presented in Fig. 4 permit tracing the specific features of shape recovery characteristics vs loading strain using various loading modes.

When using Mode 1, the recovery strain value ε_r changes in the range of 12–15.3% with a maximum at loading strain of 16%. Its value drops to 13% with the increase of loading strain as a result of the increase of the residual strain up to 4.8%. The value of total recovery strain (ε_r^{tot}) changes synchronously: its maximal value amounts to 15.7% while the minimal one is 12.6%. The TWSME value reaches its maximum of 4.2–4.6% after loading with ε_t =16–19% (see Fig. 4).

Transition to Mode 2 brings noticeable changes. The recovery strain ε_r as well as total recovery strain ε_r^{tot} gradually grow from 10 to 15% and from 12 to 17% respectively vs loading strain. The TWSME value reaches its maximum

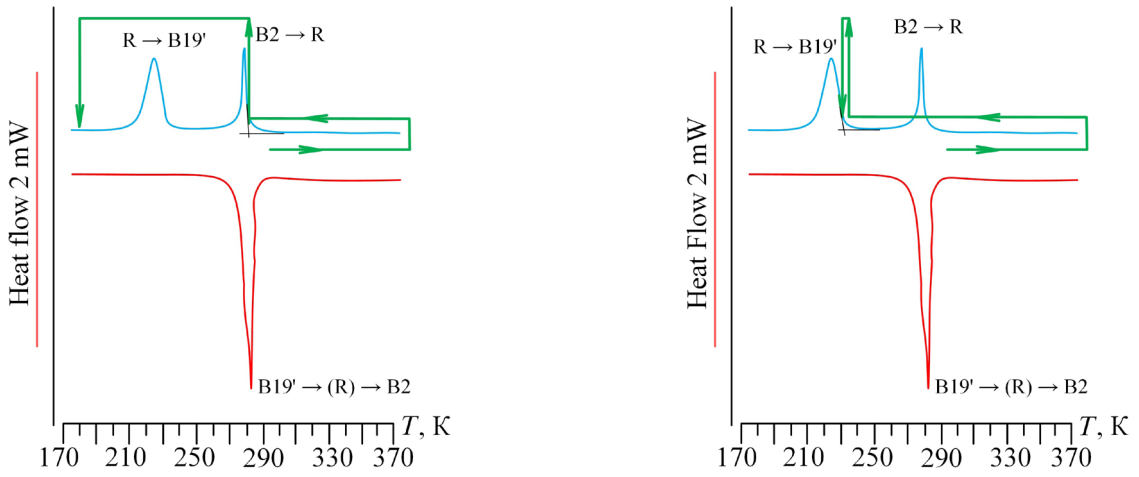

Fig. 3. (Color online) Calorimetric curves (cooling — upper, and heating — lower) after isothermal aging at 823 K for 0.5 h; green lines show temperature routs of training modes: Mode 1 (a); Mode 2 (b).

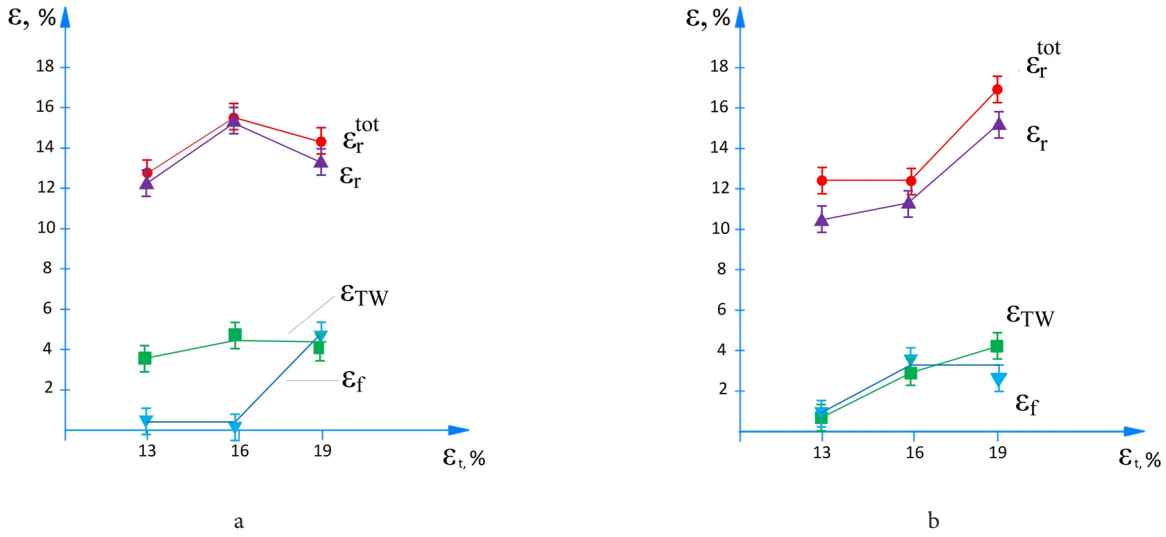

Fig. 4. (Color online) Evolution of shape recovery characteristics: Mode 1 (a); Mode 2 (b); ε_{TW} value was measured at 273 K (a) and 77 K (b).

of 4% after loading with ε_t=19% (see Fig. 4). The maximal residual strain ε_f amounts to 3.6% at ε_t=16%.

Note that the evolution character of the recovery strain and total recovery strain differs when using Modes 1 and 2. In case of Mode 1 the recovery strain evolution manifests an expressed extremum at a loading strain of 16%. When using Mode 2 the recovery strain sharply increases with the increase of loading strain from 16 to 19%. The maximum of total recovery strain (as well as the recovery strain in the present experiment is revealed under loading strain of 19% when using Mode 2. To explain the observed patterns, the mechanisms of SME inducing vs temperature must be considered; the corresponding analysis of stress-temperature behavior associated with the characteristic temperature of MTs is given in [20].

In our experiment, loading is carried out at R_s temperature (Mode 1) and M_s temperature (Mode 2). Under the applied external stress at R_s temperature (Mode 1), MT R→B19' starts at a temperature $M_s(\sigma)$ above M_s (in accordance to Clausius-Clapeyron equation). The higher the applied stress, the higher the $M_s(\sigma)$ temperature of stress-induced martensite. When the transformation yield stress is reached, the strain accumulates only through the formation of the favorably oriented stress-induced martensite, until (1) the lattice strain resource of the MT is exhausted or (2) the dislocation yield stress of martensite or austenite is reached. The stress-induced martensite stabilizes under subsequent cooling to 77 K under a constant strain.

When using Mode 2, the applied stress at M_s temperature brings the formation of the stress-induced martensite by R→B19' mechanism, which starts at a minimal stress. At R_s temperature the difference between the dislocation yield stress and transformation yield stress is significantly lower than at M_s temperature (for illustration see Fig. 4.1 in [20]). When the dislocation yield stress is reached at a certain temperature, plastic deformation starts through a dislocation slip mechanism. This deformation is irreversible. Thus, in the case of Mode 1, plastic deformation must start at a lower strain value if compared to Mode 2. The decrease of the recovery strain (see Fig. 4 a) indicates that plastic deformation already starts at 19% of loading strain. Obviously, in the case of Mode 2 the same loading strain value is not enough for reaching the dislocation yield stress. This consideration meets

with the data presented in Fig. 4 b and explains the maximal shape recovery value when using Mode 2.

In both cases, subsequent unloading results in the elastic recoil (ε_{el}) which can be evaluated as a difference between ε_r^{tot} and ε_r values (see Fig. 4). The ε_{el} does exceed 2%. After unloading the accumulated transformation strain does not disappear due to phenomena of martensitic stabilization (it will be described further on).

The above findings indicate that the maximum total recovery strain 15–17% exceeds the theoretical resource of the MT of lattice strain, which amounts 10.5% for Ni-rich titanium nickelide. According to [21], an additional mechanical twinning on {113} and {201} planes in B19'-martensite explains the physical nature of abnormally high shape recovery characteristics. (According to [22,23] the earlier revealed twining mode for R→B19' transformation is $(001)_M$). The obtained value of the recovery strain 14% somewhat higher than that of determined in the same alloy (12%) with comparable grain/subgrain size obtained as a result of aging at 703 K [24].

The plots presented in Fig. 5 permit tracing the specific features of shape recovery evolution under cooling-heating using various loading modes. In both cases, the shape recovery kinetics after unloading manifests a non-monotonic character. Partial shape recovery of 2% is observed upon heating in the range of 77–273 K, up to the inflection point at 276 K (Mode 1, Fig. 5 a) and 258 K, (Mode 2, Fig. 5 b). Upon further heating, the shape recovery proceeds more intensively.

It can be assumed that the two-stage character of shape recovery can be associated with de-twinning after twinning along {113} and {201} planes. An increase in the intensity of the shape recovery process with further heating can be associated with the predominant contribution of the reverse movement of interphase and intercrystalline boundaries.

The diagrams presented in Fig. 6 permit tracing the evolution of the shape recovery range vs loading strain using various modes. The temperature range of start and finish MTs determined from the calorimetric curves (275–285 K, see Fig. 3) is shown as well.

We could not find the difference between the temperatures of the shape recovery start, because of technical difficulties in determining the temperatures in the range of 77–258 K in

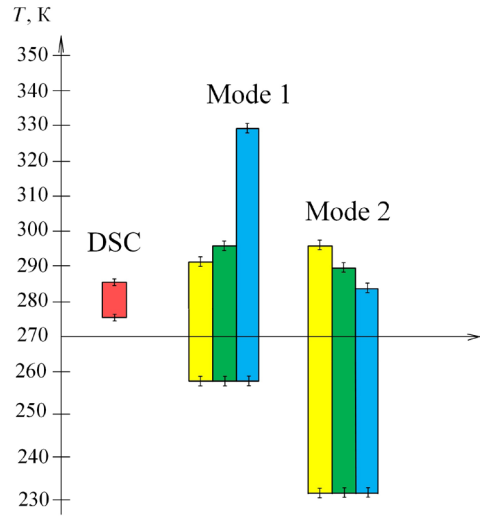

Fig. 6. (Color online) Temperature ranges of the reverse MT (A_s-A_f, red column) and shape recovery: 1st column ε_t=13%; 2nd column ε_t=16%; 3rd column ε_t=19%.

case of Mode 1. When using Mode 2, shape recovery started immediately after unloading at a temperature of 321 K.

When using Mode 1, the finish temperature of shape recovery increases sharply from 298 to 335 K vs loading strain (in the range of 13–19%), therefore the shape recovery range expands from 35 to 77 K.

The effect of loading strain on the temperature range of shape recovery is explained by the phenomenon of the martensite stabilization [25–27]. In accordance with [27], cooling of the sample in a loaded condition is accompanied by "damaging intermartensite interfaces, which form when the oriented martensite plates interact during growth upon cooling". The mobility of the interfaces decreases, therefore overheating is necessary "to provide their movement during the reverse transformation".

When using Mode 2, shape recovery proceeds in the range of lower temperatures, herewith the finish temperature of shape recovery gradually drops with the increase of loading strain from 297 to 285 K (see Fig. 6). So, the temperature range of shape recovery narrows from 66 to 54 K. The observed regularities partly correlate with the data of [26] according

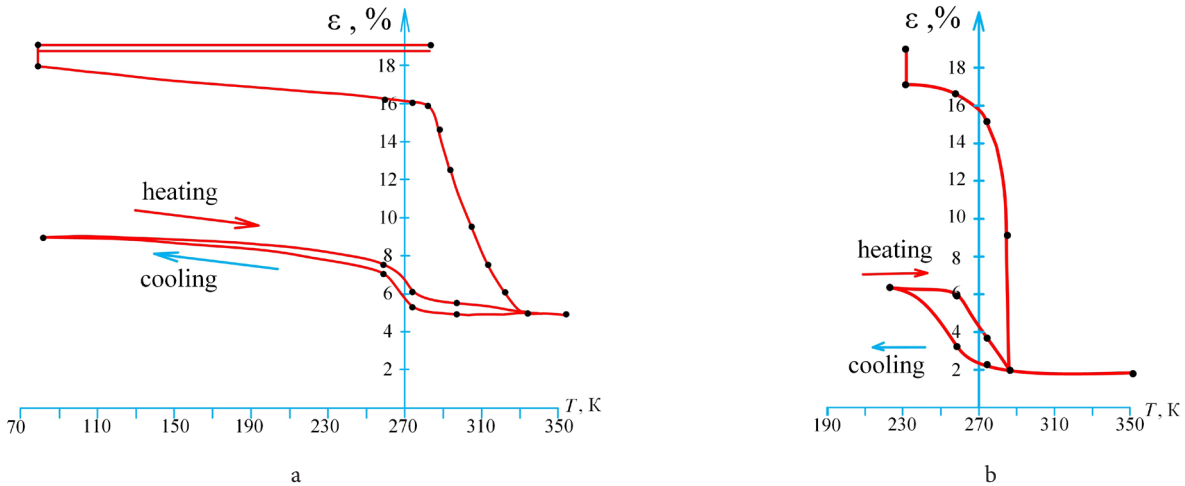

Fig. 5. (Color online) Strain-temperature curves after unloading: Mode 1 (a) and Mode 2 (b); the double line designates cooling under load.

to which "if the deformation occurs due to reorientation of the R phase, the martensite stabilization effect is negligible" if compared with the case when using Mode 1. The phenomenon of the decrease of the finish temperature of shape recovery vs loading strain and consequently narrowing of temperature range of shape recovery needs special study.

4. Conclusions

We have investigated the effect of external action, namely the initial phase state and loading strain on thermokinetics and the temperature range of shape recovery in Ni-rich titanium nickelide. The general results of the present studies can be summarized as follows:

1. Post-deformation annealing at a temperature of 823 K (30 min) after cold drawing with the accumulated logarithmic strain of 0.6 forms a mixed nano-sized grain/subgrain structure of B2 austenite; their fractions are comparable.

2. The initial phase state as well as loading strain permit the regulation of shape recovery value of Ni-rich titanium nickelide within a wide range. The highest value of total recovery strain 17% in nano-structured Ni-rich titanium nickelide is realized as a result of isothermal loading-unloading procedure at a start temperature of martensitic transformation M_s with the predominant contribution of the recovery strain of 15%.

3. The highest value of the recovery strain ε_r=15% is realized when using non-isothermal mode with a loading strain of 16% and isothermal mode with a loading strain of 19% as well as the highest TWSME value in the range of 4.1–4.5% in both cases.

4. A two-stage character of shape recovery after unloading has been revealed; a hypothesis to explain the observed phenomenon is suggested.

5. Variation of loading–unloading strain and temperature in the training procedure appears a powerful tool for controlling shape memory effects as well as thermokinetics and temperature range of shape recovery.

Acknowledgements. The work was carried out with the financial support of the Russian Science Foundation (Project No. 19-79-10270). The DSC study was performed by Prof. N. N. Resnina using the facilities of Saint-Petersburg State University (Russian Federation). The TEM characterization was carried out on the equipment of the Centre Collective Use "Materials Science and Metallurgy" with the financial support by the Ministry of Education and Science, Russia (No. 075-15-2021-696).

References

1. S. Prokoshkin, V. Brailovski, I. Khmelevskaya, K. Inaekyan, V. Demers, S. Dobatkin, E. Tatyanin. Mater. Sci. Eng. 481, 114 (2008). Crossref
2. A. Churakova, D. Gunderov, M. Kayumova. J. Phys. Conf. Ser. 1758 (1), 012008 (2021). Crossref
3. V. Komarov, I. Khmelevskaya, R. Karelin, S. Prokoshkin, M. Zaripova, M. Isaenkova, G. Korpala, R. Kawalla. J. Alloys. Compd. 797, 842 (2019). Crossref
4. E. Ryklina, S. Prokoshkin, A. Chernavina, N. Perevoshchikova. Inorg. Mater. Appl. Res. 1, 188 (2010). Crossref
5. V. Grishkov, V. Timkin, A. Lotkov, D. Zhapova. AIP Conf. Proc. 2310, 020118 (2020). Crossref
6. A. Bhardwaj, M. Ojha, A. Garudapalli, A.K. Gupta. J. Mater. Proc. Technol. 294, 117132 (2021). Crossref
7. E. Ryklina, K. Polyakova, S. Prokoshkin. Shap. Mem. Superelast. 6 (2), 157 (2020). Crossref
8. E. Ryklina, S. Prokoshkin, K. Vachiyan. IOP Conference Series: Mater. Sci. Eng. 63, 902 (2014). Crossref
9. A. Razov, A. Motorin, G. Nakhatova. J. Alloys Compd. 577, 164 (2013). Crossref
10. E. Ostropiko, Yu. Konstantinov. J. Mater. Sci. and Technol. 37, 794 (2017). Crossref
11. J. Mohd Jani, M. Leary, A. Subic, M.A. Gibson. Mater. Des. 56, 1078 (2014). Crossref
12. E.P. Ryklina, I.Yu. Khmelevskaya, S.D. Prokoshkin, K.E. Inaekyan, R.V. Ipatkin. Mater. Sci. Eng. A. 438–440, 1093 (2006). Crossref
13. E.P. Ryklina, I.Yu. Khmelevskaya, S.D. Prokoshkin. Met. Sci. Heat Treat. 46 (5-6), 179 (2004). Crossref
14. I.Yu. Khmelevskaya, E.P. Ryklina, S.D. Prokoshkin, G.A. Markossian, E.P. Tarutta, E.N. Iomdina. Mater. Sci. Eng. A. 481–482 (1–2 C), 651 (2008). Crossref
15. K. Polyakova, E. Ryklina, S. Prokoshkin. Shape Mem. Superelast. 6 (1), 139 (2020). Crossref
16. T. Poletika, S. Girsova, A. Lotkov, K. Krukovskii. Tech. Phys. 6 (4), 490 (2019). Crossref
17. T. Poletika, S. Girsova, A. Lotkov. Intermet. 106966, 127 (2020). Crossref
18. N. Kuranova, D. Gunderov, A. Uksusnikov, A. Luk'Yanov, L. Yurchenko, E. Prokof'Ev, V. Pushin, R. Valiev. Phys. Met. Metallogr. 108 (6), 556 (2009). Crossref
19. A.Y. Kolobova, E.P. Ryklina, S.D. Prokoshkin, K.E. Inaekyan, V. Brailovskii. Phys. Metals Metallogr. 119 (2), 134 (2018). Crossref
20. S.D. Prokoshkin. Chapter 4. In: V. Brailovski, S. Prokoshkin, P. Terriault, F. Trochu. Montreal: ETS Publ. (2003) 851 p.
21. Yu. Chumlyakov, I. Kireeva, E. Panchenko, I. Karaman, H.J. Maier, E. Timofeeva. J. Alloys Compd. 577, 393 (2013). Crossref
22. K. Madangopal, J.B. Singh. Acta Mater. 48, 1325 (2000).
23. K. Otsuka, X. Ren. Progr. Mater. Sci. 50, 511 (2005). Crossref
24. K. Polyakova, E. Ryklina, S. Prokoshkin. Materials Today: Proc. 4 (3), 4836 (2017).
25. S.D. Prokoshkin, S. Turenne, I.Yu. Khmelevskaya, V. Brailovski, F. Trochu. Can. Metall. Q. 39, 225 (2013). Crossref
26. S. Belyaev, N. Resnina, T. Rakhimov, V. Andreev. Sens. Actuators A Phys. 305, 111911 (2020). Crossref
27. S. Belyaev, N. Resnina, A. Ivanova, I. Ponikarova, E. Iaparova. Shape Mem. Superelast. 6, 223 (2020). Crossref